

Article

A Reconfigurable Local Oscillator Harmonic Mixer with Simultaneous Phase Shifting and Image Rejection

Bin Wu *, Chaoyue Zheng, Hao Zhang and Qingchun Zhao

Hebei Key Laboratory of Marine Perception Network and Data Processing, School of Computer and Communication Engineering, Northeastern University at Qinhuangdao, Qinhuangdao 066004, China; 2172195@stu.neu.edu.cn (C.Z.); 2372423@stu.neu.edu.cn (H.Z.); zhaqingchun@neuq.edu.cn (Q.Z.)

* Correspondence: wubin@neuq.edu.cn

Abstract: The multibeam high-throughput satellites (HTS) are regarded as a crucial component in the forthcoming space-based Internet of Things (S-IoT) network. The multi-band frequency conversion capability of HTS is essential for achieving high-capacity information interconnection in the S-IoT network. To enhance the frequency conversion capability of the on-board payload, a reconfigurable local oscillator (LO) harmonic mixer with simultaneous phase shifting and image-rejection is proposed and demonstrated based on a polarization division multiplexing dual-parallel Mach–Zehnder modulator (PDM-DPMZM). By adjusting the input radio frequency (RF) signal and direct current (DC) bias voltage of the modulator, four different LO frequency-multiplication mixing functions can be achieved. The phase of the generated signal can be flexibly tuned over a full 360° range by controlling the angle α between the polarization direction of the polarizer and one axis of the modulator, and it has a flat amplitude response. When combined with an optical frequency comb, the scheme can be extended to a multi-channel multi-band frequency conversion system with an independent phase tuning capability. Additionally, by adjusting the phase difference between dual channel output signals, it can be reconfigured to implement in-phase/quadrature (I/Q) mixing, double-balanced mixing and image-reject mixing.

Keywords: frequency conversion; space-based Internet of Things; microwave photonics; phase shifting



Citation: Wu, B.; Zheng, C.; Zhang, H.; Zhao, Q. A Reconfigurable Local Oscillator Harmonic Mixer with Simultaneous Phase Shifting and Image Rejection. *Electronics* **2024**, *13*, 971. <https://doi.org/10.3390/electronics13050971>

Academic Editor: Stefano Scanzio

Received: 11 January 2024

Revised: 26 February 2024

Accepted: 1 March 2024

Published: 3 March 2024



Copyright: © 2024 by the authors. Licensee MDPI, Basel, Switzerland. This article is an open access article distributed under the terms and conditions of the Creative Commons Attribution (CC BY) license (<https://creativecommons.org/licenses/by/4.0/>).

1. Introduction

As an inevitable trend in mobile communication, the space-based Internet of Things (S-IoT) is expected to play a significant role in constructing information networks across space, air, ground, and ocean [1]. Compared to conventional satellites, multiband high-throughput satellites (HTS) offer high bandwidth and propagation loss, making them a key component in the upcoming S-IoT. However, with the rapid development of K-above (Ka)/Q/V and millimeter-wave (mmWave) HTS, electrical domain processing methods are increasingly unable to meet the multi-band frequency conversion requirements of satellite payloads. Recent studies focused on photonics-based microwave frequency mixing, since it has the potential to provide high mixing performance [2].

The frequency mixing function is an essential feature of electronic receiving and transmitting systems for satellite payloads. Mixers can convert signals from different frequency bands to meet the demand of multi-band signal processing onboard. With the development of microwave photonics technology, various microwave photonics mixing schemes have been proposed [3–5]. Li et al. proposed a reconfigurable mixer based on a single polarization division multiplexing dual-parallel Mach–Zehnder modulator (PDM-DPMZM) which performs a carrier suppression single sideband (CS-SSB) signal generator without using any filters [3]. Jia and Ma designed a dual-output microwave photonic frequency converter using a 90° optical hybrid coupler [4]. Huang et al. experimentally

demonstrated a photonic microwave downconverter based on a dual-parallel MZM (DP-MZM) and a digital signal post-processing algorithm [5]. The above scheme only utilizes the first-order LO harmonic sidebands for frequency mixing. However, to obtain frequency-converted signals in different bands, multiple LO signals of different frequencies are required, and will definitely lead to increased system complexity, reduced flexibility, and higher costs. In contrast, the reconfigurable LO harmonic mixer allows for the flexible selection of appropriate LO harmonic sidebands to participate in frequency conversion, thereby effectively reducing the demand for LO signal frequencies.

The control of the signal phase is a prerequisite for achieving image rejection and is crucial in microwave photonic signal processing. Therefore, phase shifting with 360° full-range tuning capability is one of the core functions in various signal processing applications, such as IoT [6], multifunctional radars [7], and satellite payloads [8]. However, some of the current mixing schemes can only convert frequency without phase shifting [4,9,10]. Therefore, microwave photonic mixers that possess phase shifting functionalities have become a research hotspot. The previously reported schemes typically implement the phase shift function through three main approaches: adjusting the bias voltage of the modulator [11–13], adding a phase modulator (PM) [14], or utilizing polarization-based methods [3,15,16]. For instance, Chen et al. achieved the phase shifting function of the mixer by controlling the bias voltage of the modulator, but this method is susceptible to DC bias drift [11]. In reference [14], the phase shifting function is achieved by incorporating a PM after a PDM-DPMZM. However, when expanded to a multi-channel independent phase tuning system, each channel requires the addition of a PM, which increased complexity and cost. Our scheme is proposed without any additional modulators, since it generates multiple phase-shifted signals by increasing the number of polarizers (Pol) instead of modulators. In addition, the scheme will not be affected by DC bias drift, thus effectively reducing system complexity and improving frequency conversion efficiency.

Moreover, due to the complexity of the electromagnetic environment in space, the signals received by satellite antennas contains the image (IM) frequency signal corresponding to the radio frequency (RF) signal. If the mixer does not have image rejection capability, the IM signal will also generate a same-frequency intermediate frequency (IF) signal after passing through the mixing system. This IF signal would overlap with the required IF signal generated by the RF signal, which will be impossible to filter out and cause severe interference to subsequent processing. Therefore, image-reject mixer (IRM) is required to achieve image-reject mixing. The 90° -degree phase differences have been incorporated using a 90° optical hybrid coupler [4,17,18]. Nevertheless, the manufacturing process of the 90° optical hybrid coupler inherently introduces phase deviations that cannot be easily compensated, resulting in poor image-rejection performance and a low image-rejection ratio (IRR). In spite of this, a mixer with a 360° full-range phase shifting capability can generate two down-converted signals with orthogonal phases, which can effectively solve this problem. Therefore, the 360° full-range phase shifting capability in the proposed scheme is crucial for improving the image rejection performance.

In summary, a novel reconfigurable LO harmonic mixer with phase shifting and image rejection is proposed. Through reconfiguration, the sub-Y-DPMZM can generate ± 1 , ± 2 , ± 3 , or ± 4 -order LO harmonic sidebands or optical frequency combs (OFCs) separately. The sub-X-DPMZM operates in the CS-SSB mode to load the signal that requires frequency conversion. The two orthogonal polarized waves output from the PBC are converted from linear to circular polarization by adjusting the polarization controller (PC). The 360° full-range phase tuning function is realized by introducing Pol. By controlling the angles of the two Pols, the phase difference in the two down-converted signals is set to 90° , and finally input into the 90° electrical hybrid coupler to achieve the image rejection. The numerical analysis and simulation verification of the proposed scheme is conducted, and parameters such as frequency conversion gain, IRR, noise figure (NF), and spurious-free dynamic range (SFDR) are tested. The results show that the scheme can achieve four different LO harmonic mixings, and the phase can be flexibly tuned in the range of 0 to 360° . In the case of the

second-order LO harmonic down-conversion mode, the frequency conversion gain can reach over -35 dB, the IRR is 51.35 dB, and the SFDR is $97.27 \text{ dB}\cdot\text{Hz}^{2/3}$. Compared with other microwave photonic-mixing schemes, the proposed scheme has certain advantages in terms of bandwidth coverage, spurious rejection, and image rejection capabilities.

2. Principle of Operation

The schematic diagrams of the proposed scheme are shown in Figure 1. It mainly consists of a laser diode (LD), a PDM-DPMZM, a PC, a Pol, a wavelength selective switch (WSS), a polarization beam combiner (PBC), a polarization beam splitter (PBS), a 90° electrical hybrid coupler, an erbium-doped fiber amplifier (EDFA), and a photodetector (PD).

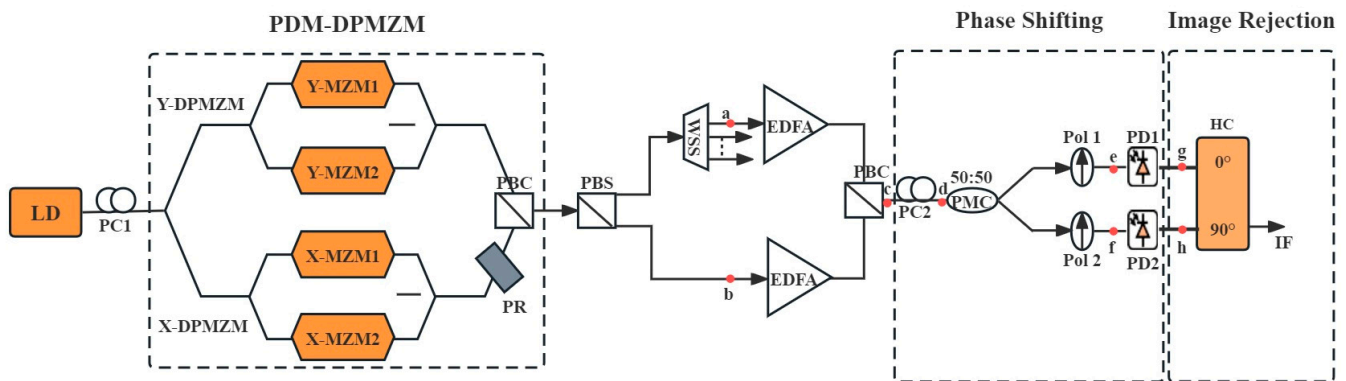


Figure 1. Schematic diagram of the reconfigurable LO harmonic mixer.

A linearly polarized light wave is emitted from a tunable laser source (TLS) and directed to the PDM-DPMZM through PC1. The PDM-DPMZM consists of a power splitter, two DP-MZMs arranged in parallel, a 90-degree polarization rotator, and a PBC. The 90-degree polarization rotator ensures that the optical signals from the upper and lower DP-MZM outputs are in orthogonal polarization states. In this scheme, the Y-DPMZM is reconfigured by adjusting the RF input and bias voltages to generate the LO \pm first, \pm second, \pm third, and \pm fourth-order harmonic sidebands, as well as the OFC. Simultaneously, the X-DPMZM operates in CS-SSB mode by setting the appropriate bias voltage.

The output optical signals from the PDM-DPMZM are divided into two orthogonal polarization states by a PBS. The upper branch's optical LO harmonic sidebands that participate in the frequency conversion are carefully selected by a WSS. Subsequently, the amplified optical signals from both the upper and lower paths are combined via a PBC to generate two linearly polarized light waves with distinct wavelengths and orthogonal polarization states. The two orthogonal linearly polarized waves are converted to two orthogonal circularly polarized waves via the adjustment of PC2. Then, the optical signal is split into two equal parts by a 50:50 polarization-maintaining coupler (PMC). By adjusting the angle between the polarization direction of the Pol and one axis of the modulator, two frequency-converted signals can be generated with a 360° range of phase tuning in a dual-channel after detection with a PD. This approach allows for the double-balanced mixing or I/Q mixing functionality to be achieved when the angular difference between the upper and lower polarizer reaches a certain value. Additionally, an electrical hybrid coupler (HC) with a 90° phase difference can be added to the I/Q mixer to achieve image rejection in down-conversion mode.

2.1. Reconfigurable LO Harmonic Sideband of Mixer

The key to achieving the LO harmonic mixer is the generation of LO harmonic sidebands of different orders. In the PDM-DPMZM configuration, the Y-DPMZM is utilized to generate LO harmonic sidebands. The LO harmonic sidebands of \pm first, \pm second, \pm third or \pm fourth-order can be selectively retained by reconfiguring the system. Meanwhile, the X-DPMZM is employed to modulate the received RF signal. This is accomplished

by adjusting the bias voltage and RF signal, which are then injected into X-MZM1 and X-MZM2 through a 90° electrical hybrid coupler. As a result, the system operates in CS-SSB mode, retaining only the +first order RF signal sideband.

To implement the LO harmonic mixing of the ±first, ±second, ±third, and ±fourth-order, the microwave signal input and DC bias of the PDM-DPMZM are illustrated in Figure 2a–c. The output of the laser diode can be expressed as $E_{in}(t) = E_c \exp(j\omega_c t)$, where E_c and ω_c are its amplitude and angular frequency, respectively.

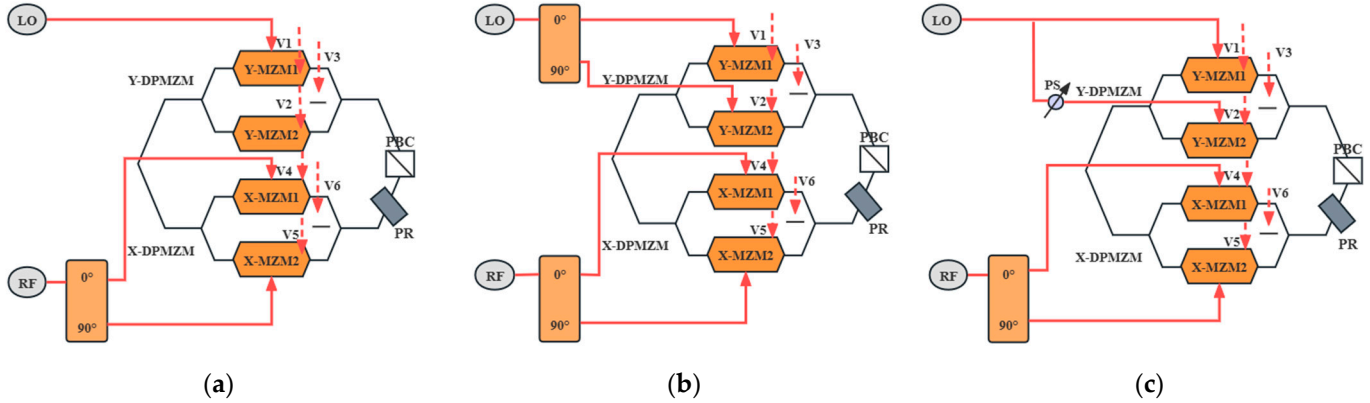


Figure 2. RF input and DC biases of PDM-DPMZM under different phase-shift functions. (a) ±first-order LO harmonic mixing; (b) ±second and ±fourth-order LO harmonic mixing; (c) ±third-order LO harmonic mixing.

Taking the generation of ±second, ±third, and ±fourth-order LO harmonic sidebands as an example., when generating the ±second-order LO harmonic sidebands, the LO signal is injected into Y-MZM1 and Y-MZM2, respectively, through the 90° electric hybrid coupler. Assuming that the LO signal is $V_{LO}(t) = V_{LO} \sin(\omega_{LO} t)$, where V_{LO} and ω_{LO} represent the amplitude and frequency of the LO signal. The LO signals injected into Y-MZM1 and Y-MZM2 are $V_{LO} \sin(\omega_{LO} t)$ and $V_{LO} \sin(\omega_{LO} t + \frac{\pi}{2})$, respectively. The output of Y-DPMZM can be expressed as

$$E_{Y-DPMZM}(t) = \frac{E_{in}(t)}{8} \left\{ \begin{array}{l} \left[\begin{array}{l} \exp(jm_{LO} \sin \omega_{LO} t) + \\ \exp(-jm_{LO} \sin \omega_{LO} t) \exp(j\theta_1) \end{array} \right] + \\ \left[\begin{array}{l} \exp(jm_{LO} \sin(\omega_{LO} t + \frac{\pi}{2})) + \\ \exp(-jm_{LO} \sin(\omega_{LO} t + \frac{\pi}{2})) \exp(j\theta_2) \end{array} \right] \exp(j\theta_3) \end{array} \right\} \quad (1)$$

where $m_{LO} = \frac{\pi V_{LO}}{V_{\pi}}$ is the modulation depth of the signal in the sub-MZMs, V_{π} is the half wave voltage of the PDM-DPMZM, and $\theta_n = \frac{\pi V_n}{V_{\pi}}$ ($n = 1, 2, 3$) are the phase changes introduced by the DC bias voltage V_n . By setting $\theta_1 = \theta_2 = 0$ and $\theta_3 = \pi$, ±second-order LO harmonic sidebands are obtained. Equation (1) can be expanded by the Bessel function as

$$E_{Y-DPMZM}(t) = \frac{E_{in}(t)}{4} \left\{ \begin{array}{l} \left[\sum_{n=-\infty}^{\infty} J_{2n}(m_{LO}) \exp(j2n\omega_{LO} t) \right] - \\ \left[\sum_{n=-\infty}^{\infty} J_{2n}(m_{LO}) \exp(j2n\omega_{LO} t) \exp(jn\pi) \right] \end{array} \right\} \quad (2)$$

$$\approx \frac{E_{in}(t)}{2} \{ [J_2(m_{LO}) \exp(j2\omega_{LO} t) + J_{-2}(m_{LO}) \exp(-j2\omega_{LO} t)] \}$$

Only the ±second-order LO harmonic sidebands are retained, and the other sidebands are suppressed.

To generate the ±third-order LO harmonic sidebands, one of the LO signals is directly injected into Y-MZM1, while the other LO signal is first phase-shifted by an electrical phase shifter and then injected into Y-MZM2. Assuming that the LO signal is represented as $V_{LO}(t) = V_{LO} \sin(\omega_{LO} t)$, the LO signals injected into Y-MZM1 and Y-MZM2

are $V_{LO} \sin(\omega_{LO}t)$ and $V_{LO} \sin(\omega_{LO}t + \varphi)$, respectively. The output of Y-DPMZM can be expressed as:

$$E_{Y-DPMZM}(t) = \frac{E_{in}(t)}{8} \left\{ \begin{array}{l} \left[\exp(jm_{LO} \sin \omega_{LO}t) + \exp(-jm_{LO} \sin \omega_{LO}t) \exp(j\theta_1) \right]^+ \\ \left[\exp(jm_{LO} \sin(\omega_{LO}t + \varphi)) + \exp(-jm_{LO} \sin(\omega_{LO}t + \varphi)) \exp(j\theta_2) \right] \exp(j\theta_3) \end{array} \right\} \quad (3)$$

When setting $\theta_1 = \theta_2 = \pi$ and $\theta_3 = 0$, \pm third-order LO harmonic sidebands are obtained. Equation (3) can be expanded using the Bessel function as:

$$E_{Y-DPMZM}(t) = \frac{E_{in}(t)}{4} \left\{ \begin{array}{l} \left[\sum_{n=-\infty}^{\infty} J_{2n+1}(m_{LO}) \exp(j(2n+1)\omega_{LO}t) \right]^+ \\ \left[\sum_{n=-\infty}^{\infty} J_{2n+1}(m_{LO}) \exp(j(2n+1)\omega_{LO}t) \exp(j(2n+1)\varphi) \right] \end{array} \right\} \quad (4)$$

When the conditions $J_1(m_{LO}) = 0$ and $1 + \exp(\pm j5\varphi) = 0$ are satisfied, \pm first-order and \pm fifth-order LO harmonic sidebands are suppressed. After performing the calculation, it is found that when $m_{LO} = 3.868$ and $\varphi = 36^\circ$, the equation mentioned above is satisfied. As a result, only the \pm third-order LO harmonic sidebands are retained, while the other sidebands are effectively suppressed.

When utilizing \pm fourth-order LO harmonic sidebands for mixing, the LO and RF signal input to the PDM-DPMZM follows a similar approach as the \pm second-order LO harmonic sideband mode, which will not be discussed in detail here. By satisfying the conditions $J_0(m_{LO}) = 0$ and $J_2(m_{LO})(1 + \exp(\pm j2\varphi)) = 0$, both the carrier and \pm second-order LO harmonic sidebands are effectively suppressed, allowing only the \pm fourth-order LO harmonic sidebands to be retained. After calculation, when $m_{LO} = 2.405$ and $\varphi = 90^\circ$, the above equation is satisfied. Furthermore, if the Y-DPMZM is utilized to generate a flat OFC, this approach can be extended to a multi-channel multi-band frequency-conversion and phase-shifting system. By modifying the configuration of the Y-DPMZM to generate different types of LO sidebands, various frequency conversion requirements can be met, thereby expanding the application range of the system.

2.2. Reconfigurable LO Harmonic Mixer with Phase Shifting and Image-Rejection Ability

All of the aforementioned four structures are capable of generating frequency-conversion and phase shifting signals, while also possessing reconfigurable mixing functions. These functions are demonstrated using the generation of \pm second-order LO harmonic sidebands as an example. Y-DPMZM generates \pm second-order LO harmonic sidebands in the y polarization direction, and the +second-order LO harmonic sideband is selected by the WSS. The output signal can be expressed as

$$E_{out-a}(t) = \frac{E_{in}(t)}{2} J_2(m_{LO}) \exp(j2\omega_{LO}t) \quad (5)$$

The X-DPMZM generates only the +first-order RF signal sideband in the x polarization direction. The output of point b can be expressed as

$$E_{out-b}(t) = \frac{E_{in}(t)}{2} J_1(m_{RF}) \exp(j\omega_{RF}t) \quad (6)$$

After passing through a PBC, the output signal can be expressed as

$$E_{out-c}(t) = \frac{E_{in}(t)}{2} J_1(m_{RF}) \exp(j\omega_{RF}t)x + \frac{E_{in}(t)}{2} J_2(m_{LO}) \exp(j2\omega_{LO}t)y \quad (7)$$

The two orthogonal line polarization wavelengths are adjusted by a polarization controller to obtain the orthogonal circular polarization wavelengths.

For forward-incident light, the transfer function of PC2 can be expressed as

$$F = \begin{bmatrix} \cos \theta & -\sin \theta \\ \sin \theta & \cos \theta \end{bmatrix} \begin{bmatrix} \exp(j\frac{\Delta}{2}) & 0 \\ 0 & \exp(-j\frac{\Delta}{2}) \end{bmatrix} \quad (8)$$

In this Equation (8), θ is the rotation angle of PC2, Δ is the phase difference caused by birefringence in PC. When $\theta = 45^\circ$ and $\Delta = \frac{\pi}{2}$, the output signal at point d after adjusting PC2 can be expressed as

$$E_{\text{out-d}}(t) = \frac{\sqrt{2}}{4} E_{\text{in}}(t) \left\{ \begin{array}{l} J_1(m_{\text{RF}}) \exp(j\omega_{\text{RF}}t) [\exp(j\frac{\pi}{4})x' + \exp(-j\frac{\pi}{4})y'] + \\ J_2(m_{\text{LO}}) \exp(j2\omega_{\text{LO}}t) [-\exp(j\frac{\pi}{4})x' + \exp(-j\frac{\pi}{4})y'] \end{array} \right\} \quad (9)$$

Then, the optical signal is divided into two equal parts using a 50:50 polarization-maintaining coupler. Through Pol1 and Pol2, these two parts are combined in the same direction with angles α_1 and α_2 , respectively. The resulting output signal can be expressed as

$$\begin{aligned} E_{\text{out-e}}(t) &= \frac{\sqrt{2}}{8} E_{\text{in}}(t) \left\{ \begin{array}{l} J_1(m_{\text{RF}}) \exp(j\omega_{\text{RF}}t - j\frac{\pi}{4}) [\exp(j\frac{\pi}{2}) \sin \alpha_1 + \cos \alpha_1] + \\ J_2(m_{\text{LO}}) \exp(j2\omega_{\text{LO}}t - j\frac{\pi}{4}) [-\exp(j\frac{\pi}{2}) \sin \alpha_1 + \cos \alpha_1] \end{array} \right\} \\ &= \frac{\sqrt{2}}{8} E_{\text{in}}(t) \left\{ \exp(-j\frac{\pi}{4}) \begin{bmatrix} J_1(m_{\text{RF}}) \exp(j\omega_{\text{RF}}t + j\alpha_1) \\ + J_2(m_{\text{LO}}) \exp(j2\omega_{\text{LO}}t - j\alpha_1) \end{bmatrix} \right\} \end{aligned} \quad (10)$$

$$\begin{aligned} E_{\text{out-f}}(t) &= \frac{\sqrt{2}}{8} E_{\text{in}}(t) \left\{ \begin{array}{l} J_1(m_{\text{RF}}) \exp(j\omega_{\text{RF}}t - j\frac{\pi}{4}) [\exp(j\frac{\pi}{2}) \sin \alpha_2 + \cos \alpha_2] + \\ J_2(m_{\text{LO}}) \exp(j2\omega_{\text{LO}}t - j\frac{\pi}{4}) [-\exp(j\frac{\pi}{2}) \sin \alpha_2 + \cos \alpha_2] \end{array} \right\} \\ &= \frac{\sqrt{2}}{8} E_{\text{in}}(t) \left\{ \exp(-j\frac{\pi}{4}) \begin{bmatrix} J_1(m_{\text{RF}}) \exp(j\omega_{\text{RF}}t + j\alpha_2) \\ + J_2(m_{\text{LO}}) \exp(j2\omega_{\text{LO}}t - j\alpha_2) \end{bmatrix} \right\} \end{aligned} \quad (11)$$

The expressions of the output current of the two-phase shifters are

$$I_{\text{AC1}}(t) \propto |E_{\text{in}}(t)| J_1(m_{\text{RF}}) J_2(m_{\text{LO}}) \times \cos[(\omega_{\text{RF}} - 2\omega_{\text{LO}})t + 2\alpha_1] \quad (12)$$

and

$$I_{\text{AC2}}(t) \propto |E_{\text{in}}(t)| J_1(m_{\text{RF}}) J_2(m_{\text{LO}}) \times \cos[(\omega_{\text{RF}} - 2\omega_{\text{LO}})t + 2\alpha_2] \quad (13)$$

From Equations (12) and (13), it can be seen that the generation of the LO multiplication down-conversion shift signal is achieved in the dual channel. By simply controlling the angles between the polarizer and one principal axis of the PDM-DPMZM, the phases of the two IF signals can be independently and continuously tuned. When the conditions $\alpha_1 - \alpha_2 = 45^\circ$ or $\alpha_1 - \alpha_2 = 90^\circ$ are satisfied, I/Q mixing or double-balanced mixing can be realized separately. Image-reject mixing is achieved by adding a 90-degree electrical hybrid coupler on the basis of I/Q mixing. In the case of the image signal, the signal before PC2 can be expressed as

$$E_{\text{out-c}}(t) = \frac{E_{\text{in}}(t)}{2} [J_1(m_{\text{RF}}) \exp(j\omega_{\text{RF}}t) + J_1(m_{\text{IM}}) \exp(j\omega_{\text{IM}}t)]x + \frac{E_{\text{in}}(t)}{2} J_2(m_{\text{LO}}) \exp(j2\omega_{\text{LO}}t)y \quad (14)$$

After photoelectric conversion by PD1 and PD2, the dual-channel output can be expressed as

$$I_{\text{AC1}}(t) \propto |E_{\text{in}}(t)| \left\{ \begin{array}{l} J_1(m_{\text{RF}}) J_2(m_{\text{LO}}) \times \cos[(\omega_{\text{RF}} - 2\omega_{\text{LO}})t + 2\alpha_1] + \\ J_1(m_{\text{IM}}) J_2(m_{\text{LO}}) \times \cos[(2\omega_{\text{LO}} - \omega_{\text{IM}})t - 2\alpha_1] \end{array} \right\} \quad (15)$$

and

$$I_{AC2}(t) \propto |E_{in}(t)| \left\{ \begin{array}{l} J_1(m_{RF})J_2(m_{LO}) \times \cos[(\omega_{RF} - 2\omega_{LO})t + 2\alpha_2] + \\ J_1(m_{IM})J_2(m_{LO}) \times \cos[(2\omega_{LO} - \omega_{IM})t - 2\alpha_2] \end{array} \right\} \quad (16)$$

If the angles are set as $\alpha_1 = 45^\circ$ and $\alpha_2 = 0^\circ$, and the two signals from the detector are coupled via a 90-degree electrical hybrid coupler, the output signal can be expressed as

$$I_{IF}(t) \propto I_{AC1}(t) + I_{AC2}(t) \exp(j\frac{\pi}{2}) \propto 2|E_{in}(t)|J_1(m_{RF})J_2(m_{LO}) \times \cos[(\omega_{RF} - 2\omega_{LO})t + \frac{\pi}{2}] \quad (17)$$

The results indicate that the intensity of the IF signal extracted from the RF signal is improved, while the IF signal obtained from the IM signal is completely eliminated. Additionally, the inherent phase deviation in the 90° electrical hybrid coupler can be compensated by adjusting the angle difference α_1 and α_2 , resulting in enhanced image rejection performance. Similarly, when the WSS selects the second-order LO harmonic sideband, the system can achieve the generation of the LO multiplication up-conversion shift signal. The introduction of the WSS enhances the system's reconfigurability, flexibility, and suitability for various scenarios.

3. Simulation Analysis and Results

3.1. Simulation Setup

A simulation was conducted based on the commercial software “Optisystem15.0” to demonstrate the feasibility of the proposed scheme, as presented in Figure 3.

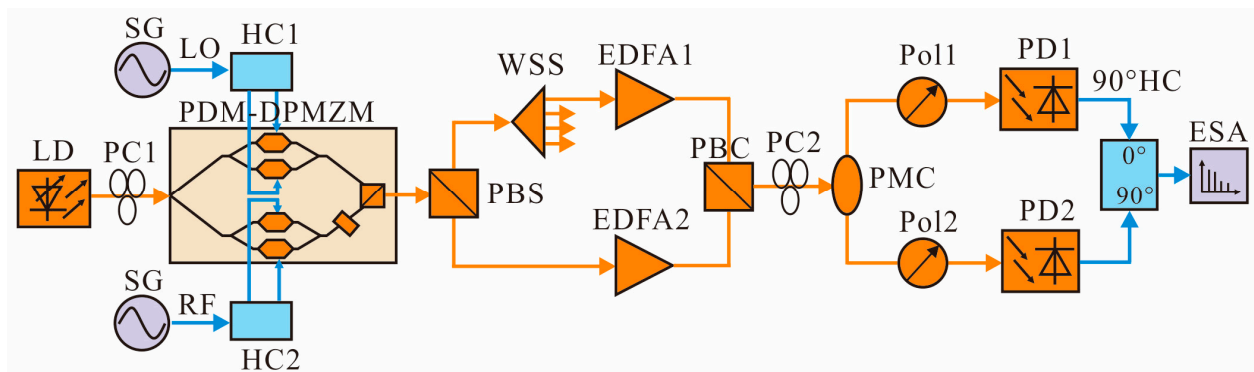


Figure 3. Setup diagram of the reconfigurable LO harmonic mixer. LD: laser diode; PC: polarization controller; SG: signal generator; LO: local oscillator; RF: radio frequency; HC: hybrid coupler; PDM-DPMZM: polarization division multiplexing dual-parallel Mach–Zehnder modulator; PBS: polarization beam splitter; WSS: wavelength selective switch; EDFA: erbium-doped fiber amplifier; PBC: polarization beam combiner; PMC: polarization-maintaining coupler; Pol: polarizer; PD: photodetector; ESA: electrical spectrum analyzer.

The optical carrier emitted from a TLS has a frequency of 193.1 THz and a power of 15 dBm. The primary device used is a PDM-DPMZM with a half-wave voltage of 3.5 V. The Y-DPMZM within it is utilized to generate various orders of LO harmonic sidebands or flat OFC in the y-polarization direction. On the other hand, the X-DPMZM operates in the CS-SSB mode in the x-polarization direction in order to load the received RF signal.

The output signal from the PDM-DPMZM is split into two signals with orthogonal polarization direction by a PBS. The required LO sidebands are selected by the WSS in the y polarization direction, and then a pair of orthogonal line polarization wavelengths are obtained through PBC combination. By adjusting the polarization controller, the orthogonal line polarization wavelength is converted to an orthogonal circular polarization wavelength, and then divided into two identical optical signals by a 50:50 polarization-maintaining coupler. By controlling the angle between the polarizer and one principal axis of the PDM-DPMZM, the phases of the generated frequency-conversion signals can be independently

and continuously tuned. The system structure is depicted in Figure 2 and the corresponding parameter settings are listed in Table 1.

Table 1. Value of RF input and DC biases under different conditions.

The out of Y-DPMZM	ω_{RF}/GHz	ω_{LO}/GHz	V_{LO}	V_1	V_2	V_3	V_{RF}	V_4	V_5	V_6
± 1 order LO Harmonic	8	5	0.7	3.5	3.5	3.5	0.5	3.5	3.5	-1.75
± 2 order LO Harmonic	18	5	2.9	0	0	3.5	0.5	3.5	3.5	-1.75
± 3 order LO Harmonic	28	5	4.311	3.5	3.5	0	0.5	3.5	3.5	-1.75
± 4 order LO Harmonic	38	5	2.681	0	0	0	0.5	3.5	3.5	-1.75
5-line LO OFC	6	5	0.925	0.455	-1.05	-2.8	0.5	3.5	3.5	-1.75
7-line LO OFC	6	5	3.395	2.205	3.22	2.555	0.5	3.5	3.5	-1.75

3.2. Results and Discussion

3.2.1. Multi-Band Frequency Conversion

To test the frequency conversion capability and reconfigurability of our LO harmonic mixing scheme, a simulation system was established. The spectra of the PDM-DPMZM output and the electrical spectrum of the PD output were measured, and the results are shown in Figure 4.

As shown in Figure 4a,b, the spectrum represented by the green line corresponds to the signal in the x-polarization direction, while the red line represents the signal in the y-polarization direction.

As illustrated in Figure 4a–f, the spectra obtained by the reconfigurable LO harmonic mixing processes exhibit a high optical spurious suppression ratio (OSSR), and the generated electrical spectra have a high spurious suppression ratio (SSR) as well. For instance, in the LO quadruplicated frequency up/down conversion process shown in Figure 4b, the OSSR is 47.4 dB and 37.9 dB in the x-polarization and y-polarization direction, respectively. Assuming that the RF signal and LO signal is 38 GHz (Ka band) and 5 GHz, respectively, the frequency of the LO quadruplicated frequency down-conversion signal becomes 18 GHz (K band) while the SSR of the electrical spectra is 39.4 dB. Similarly, the frequency of the up-conversion signal is 58 GHz (V band) with the SSR of 39.4 dB. In certain exceptional scenarios, where the received RF signal requires conversion across a wide range, higher-order schemes such as the \pm fourth-order LO harmonic can be chosen. This reduces the requirement of the LO signal frequency while meeting the diverse communication service needs.

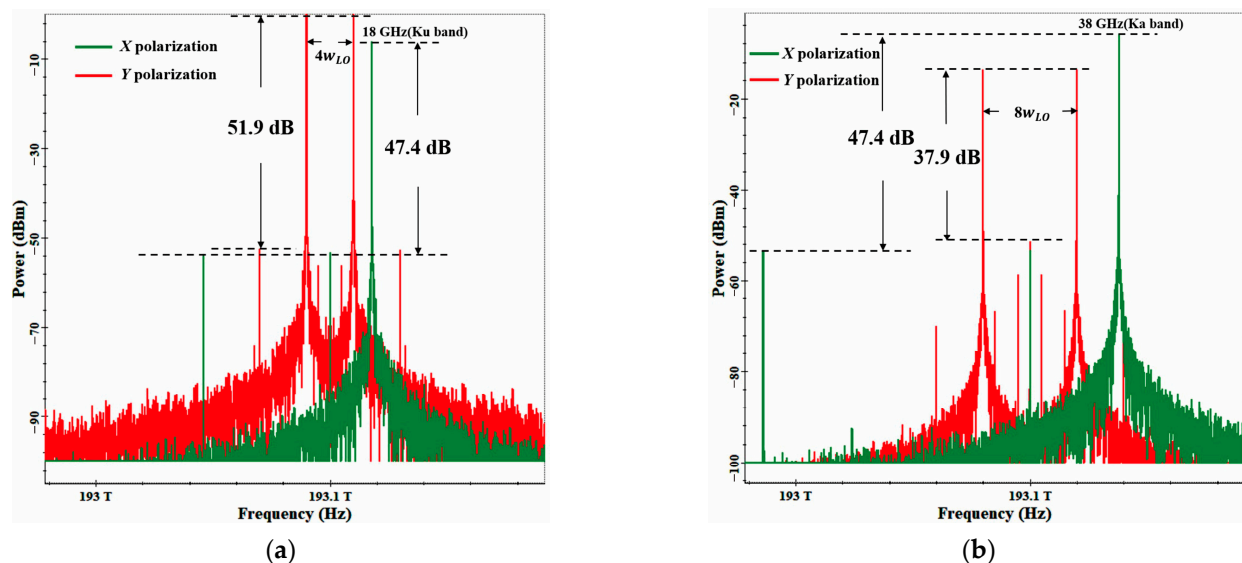


Figure 4. Cont.

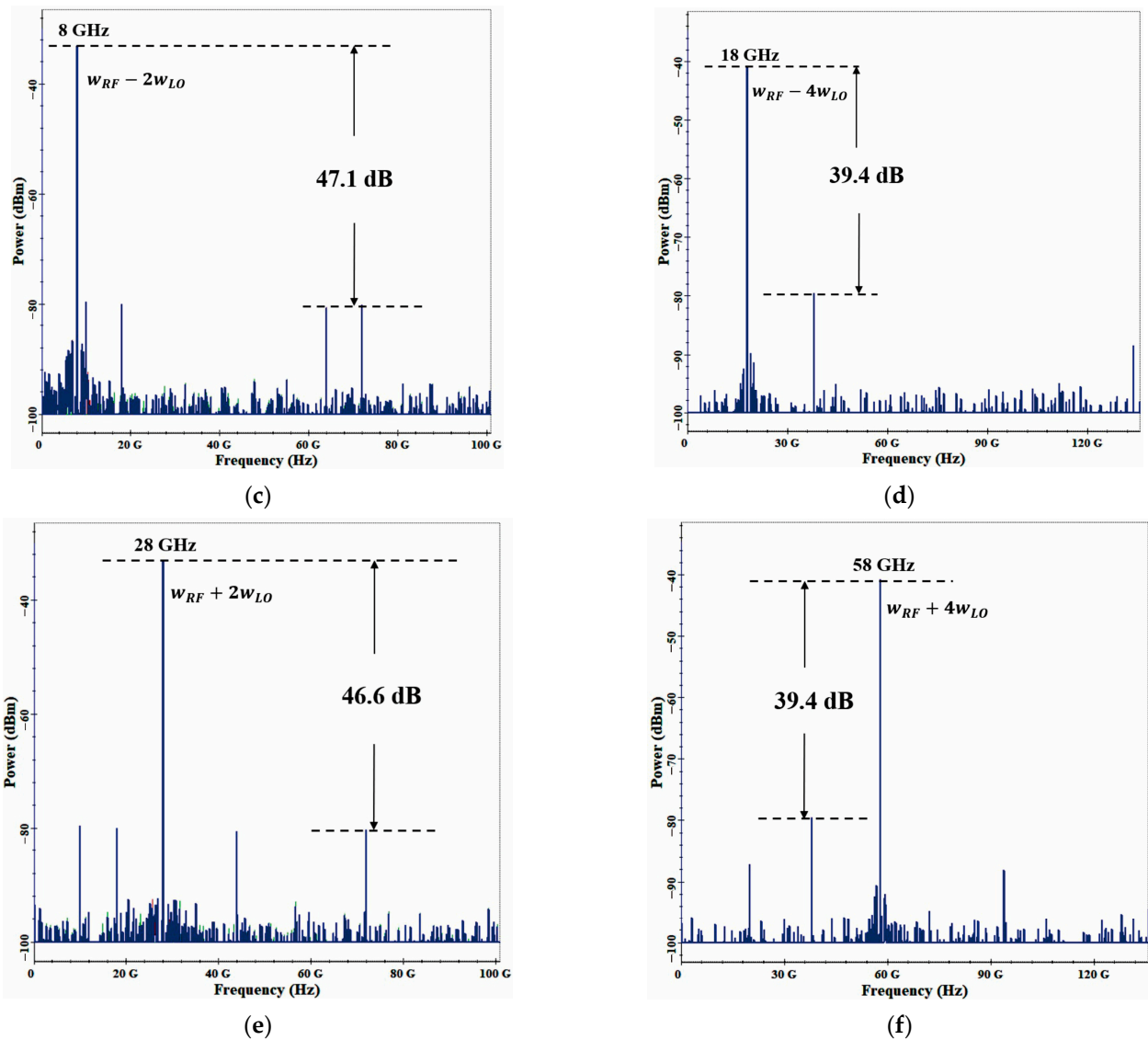


Figure 4. Optical spectra at the output of PDM-DPMZM and electric spectra at the output of PD under different LO conditions. \pm second-order LO harmonic (a,c,e); \pm fourth-order LO harmonic (b,d,f).

In multi-band frequency conversion applications, the Y-DPMZM can be configured to generate either five or seven line OFCs. In this case, it is assumed that \pm third-order optical sidebands of the seven line OFC were selected by WSS for frequency conversion. The spectrum of the PDM-DPMZM output and the corresponding electrical spectrum after conversion are shown in Figure 5a–c. The SSR of the signal after up/down conversion is higher than 42 dB, indicating good quality. In practical scenarios, the WSS can be adjusted to filter out different comb lines, resulting in different frequency conversion signals based on specific requirements.

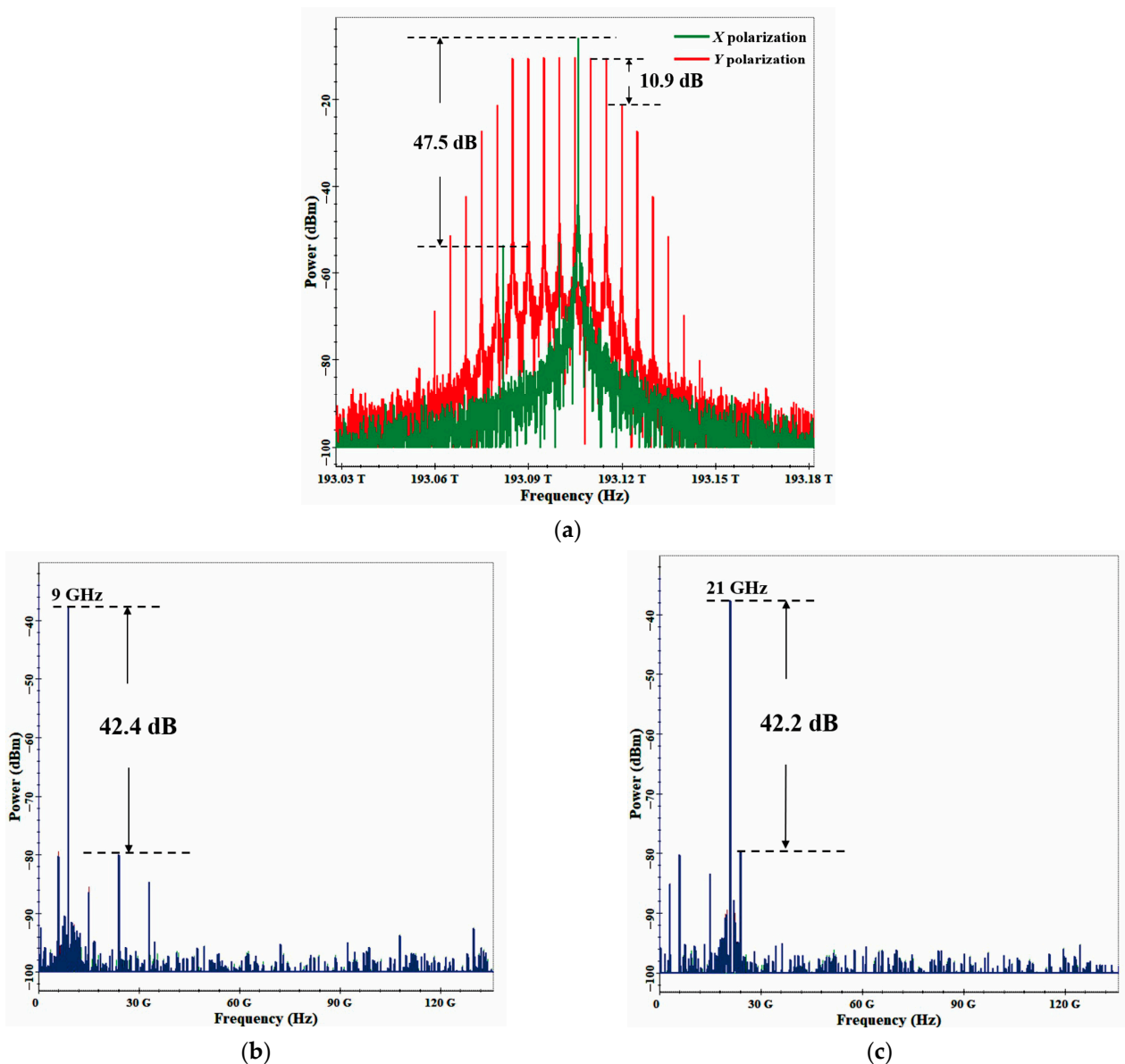


Figure 5. Optical spectra at the output of PDM-DPMZM (a) and electric spectra at the output of PD when RF signal is mixed with the +3rd-order sideband (b) or -3rd-order sideband (c) of 7-line LO OFC.

In order to verify the wide tunability of the second-order LO harmonic mixer, we tuned the RF/IF signal from 21 GHz to 30 GHz in steps of 1 GHz. For a fixed 5 GHz LO signal, an up-converted range of 31–40 GHz and a down-converted range of 11–20 GHz were realized, as shown in Figure 6a,b, respectively. It can be seen that the spurious mixing is suppressed by 46.87 dB and 49.78 dB, respectively, with high SSR. However, the SSR in [4] is only around 30 dB.

In order to verify the quality of the output signal of the second-order LO harmonic mixer, we analyzed the conversion gain and NF of the system. The power of the LO signal was set to 19.25 dBm. When the RF/IF frequency was tuned from 21 GHz to 30 GHz in 1 GHz steps, and the LO frequency was correspondingly tuned from 9 GHz to 13.5 GHz in 0.5 GHz steps, the IF frequency was fixed at 3 GHz in the down conversion. Alternatively, the LO frequency was tuned from 9.5 GHz to 5 GHz in steps of 0.5 GHz and the output RF signal frequency was fixed at 40 GHz at up conversion. The conversion gain for different RF/IF frequencies is shown in Figure 7a. It can be seen that the conversion gain is about

−34 dB, with a fluctuation of about 0.4 dB. In order to measure the NF, the frequencies of RF/IF and LO were set to 18 GHz and 5 GHz, respectively. When the power tuning range of the LO signal is from 6 dBm to 18 dBm, the NF curve is shown in Figure 7b.

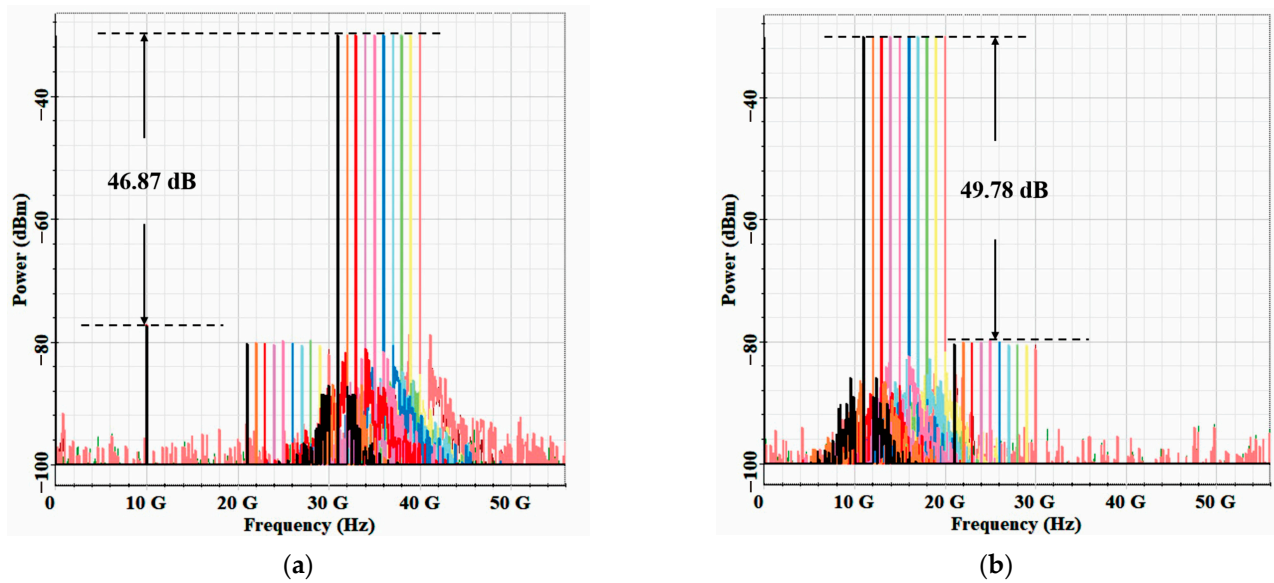


Figure 6. Electrical spectra of the mixed electrical signal of the second-order LO harmonic mixer for (a) frequency up-conversion from 31 GHz to 40 GHz and (b) frequency down-conversion from 11 GHz to 20 GHz. Different colors indicate different RF signal frequencies, varying from 21 GHz to 30 GHz in 1 GHz steps.

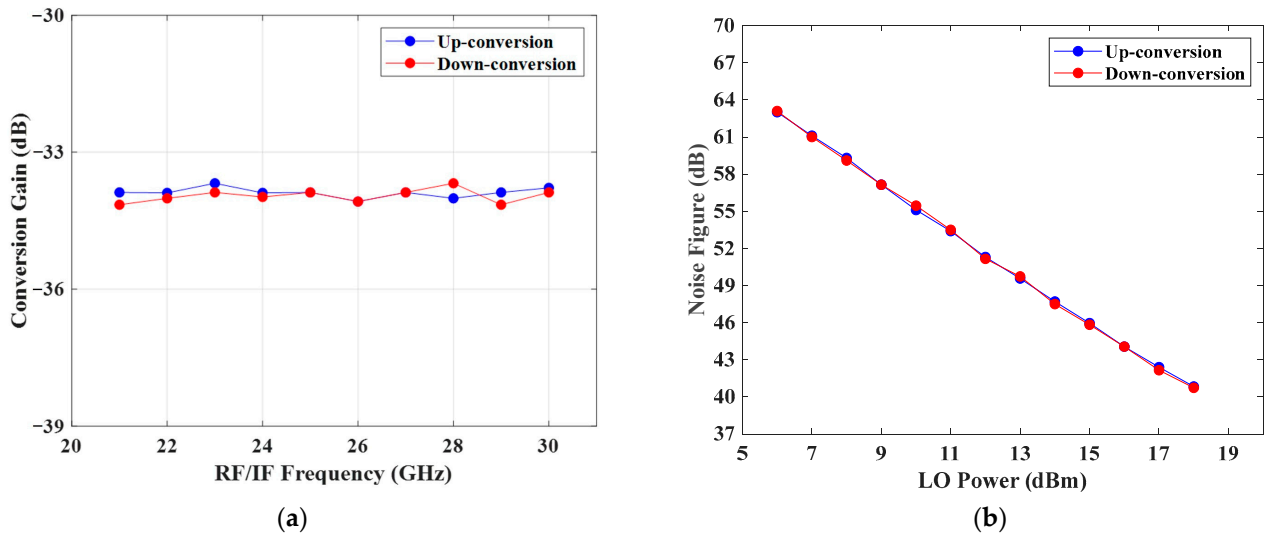


Figure 7. Conversion gain (a) and NF of the second-order LO harmonic mixer (b).

3.2.2. 360° Phase Tuning

In order to demonstrate the 360° phase tuning capability of the generated frequency conversion signal, we present the case of second-order LO harmonic mixing as an example. By simply adjusting the angle between the polarizer and one principal axis of the PDM-DPMZM, the phases of the generated frequency-conversion signals can be independently and continuously tuned. The measured waveforms of up-conversion and down-conversion signals with 360° phase tuning are shown in Figure 8a,b, respectively. The results indicate that with the change in phase, the amplitude fluctuations of the waveforms in both cases are small and have a relatively flat amplitude response.

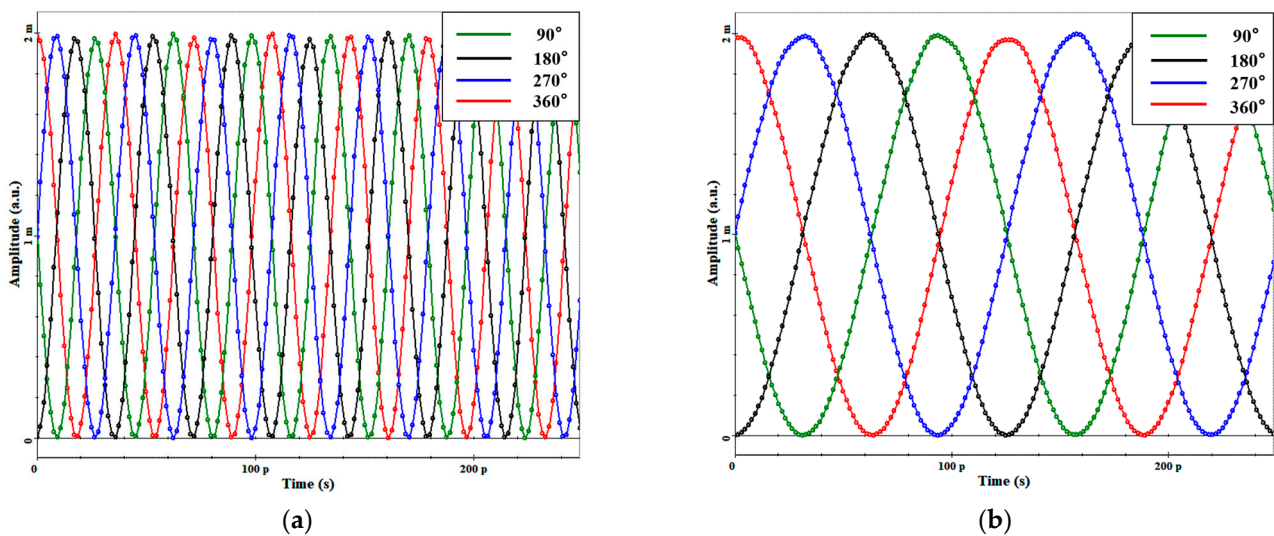


Figure 8. Waveforms of signals after phase continuous tuning in the case of the second-order LO harmonic mixing operation. (a) Up-conversion signal (28 GHz); (b) down-conversion signal (8 GHz).

Taking the second-order LO harmonic down-conversion as an example, I/Q mixing and double-balanced mixing are achieved by appropriately setting the angles of α_1 and α_2 . Specifically, when $\alpha_1 - \alpha_2 = 45^\circ$, I/Q mixing is achieved, while when $\alpha_1 - \alpha_2 = 90^\circ$, double-balanced mixing is achieved. For simplicity, we assume $\alpha_1 = 45^\circ$, $\alpha_2 = 0^\circ$ for I/Q mixing and $\alpha_1 = 90^\circ$, $\alpha_2 = 0^\circ$, for double-balanced mixing. The corresponding waveforms are shown in Figure 9a,b, respectively. It can be observed that in the case of I/Q mixing, the two waveforms have the same amplitude and 90° phase difference, whereas in the case of double-balanced mixing, the waveforms have the same amplitude but an opposite phase.

3.2.3. Image Rejection and SFDR

To validate the image-reject capability of our proposed reconfigurable LO harmonic mixer, a simulation was conducted using the second-order LO harmonic down-conversion mode. In the simulation, the LO signal frequency was set to 5 GHz, while the input RF signal and the image signal were set to 18 GHz and 2 GHz, respectively. The I/Q mixing function was implemented, and the IF signal waveforms generated by the RF signal and image signal frequency conversion are shown in Figure 10a,b, respectively.

In Figure 10a, the black and blue dashed line indicate the waveforms of the IF signal output by PD1 and PD2 after frequency conversion of RF signal, while the red and green dashed line represent the IF signal after the frequency conversion of the image signal. In order to achieve image rejection, an additional 90° electrical hybrid coupler is required on the basis of the I/Q mixing, thus introducing a 90° phase shift in the PD2 output signal. It can be seen that after the introduction of the 90° phase shift in PD2, the amplitude and phase of the two IF signal waveforms from RF signal frequency conversion are identical, and the signal strength is enhanced. Furthermore, the two IF signal waveforms obtained from the image signal conversion have the same amplitude but opposite phases, thus suppressing the interference signal generated by the image signal conversion.

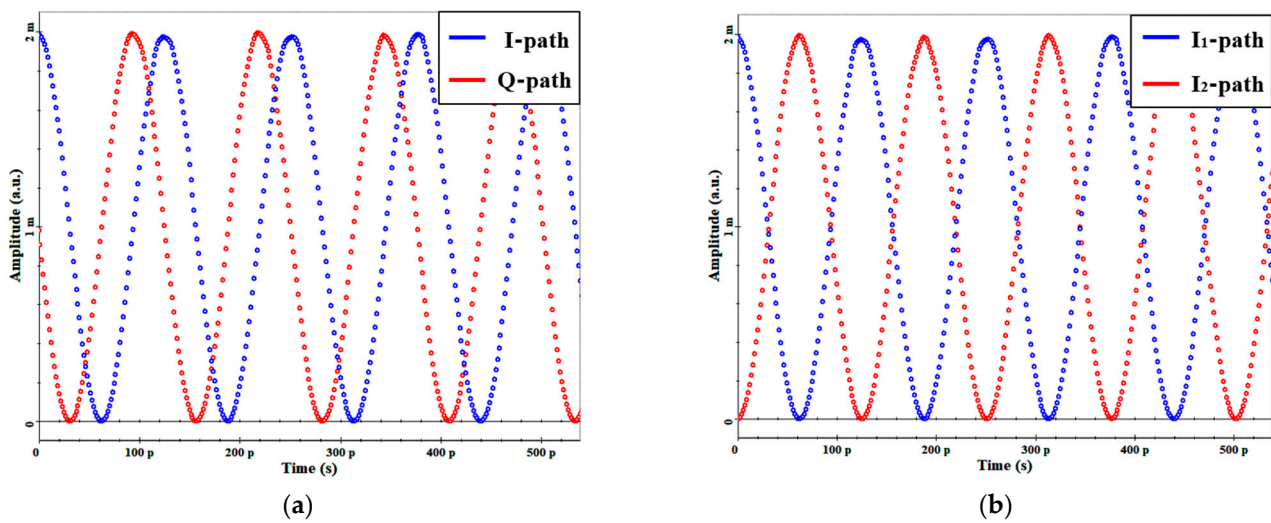


Figure 9. Waveforms of I/Q mixing and double-balanced mixing in the case of the second-order LO harmonic down-conversion. (a) I/Q mixing; (b) double-balanced mixing.

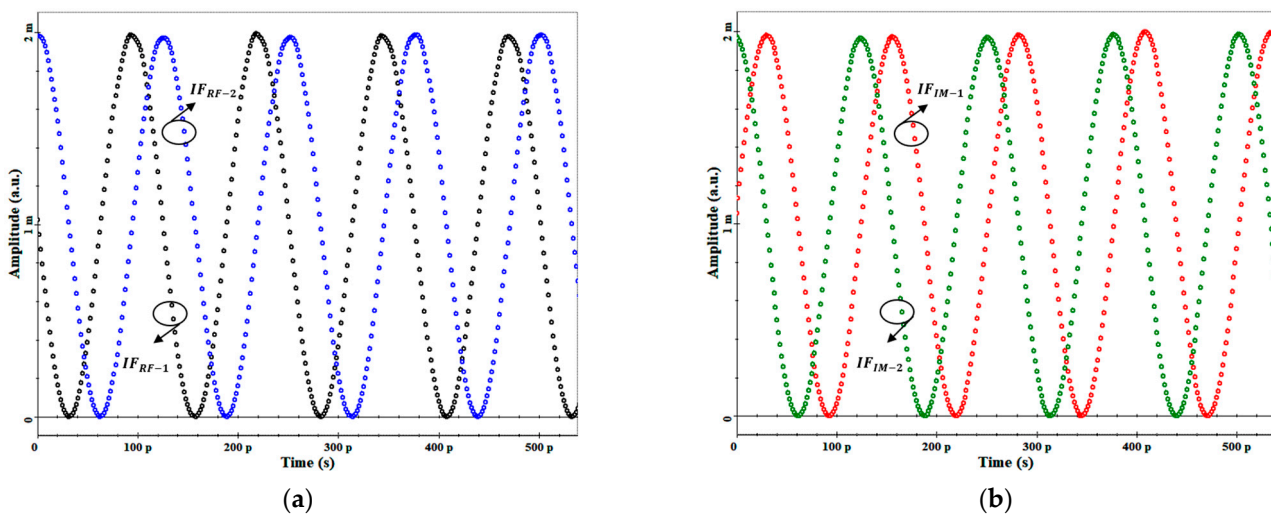


Figure 10. Waveforms of the IF signals at the outputs of PD1 and PD2 in the case of I/Q mixing. (a) The two RF-induced IF signals; (b) the two image-induced IF signals.

In the simulation, the RF signal and image signal are applied simultaneously, and the electrical spectrum and waveform of the down-converted signal are shown in Figure 11a,b, respectively. It can be observed that the IF signal generated by the image signal frequency conversion is well suppressed with an IRR of 51.35 dB as presented in Figure 11a. In the same situation without using a 90° optical hybrid coupler, the IRR is also better than the 45.91 dB in [10]. Additionally, in Figure 11b, the amplitude of the IF signal waveform generated by the frequency conversion of the image signal is almost zero. The above analysis is well supported by the simulation results.

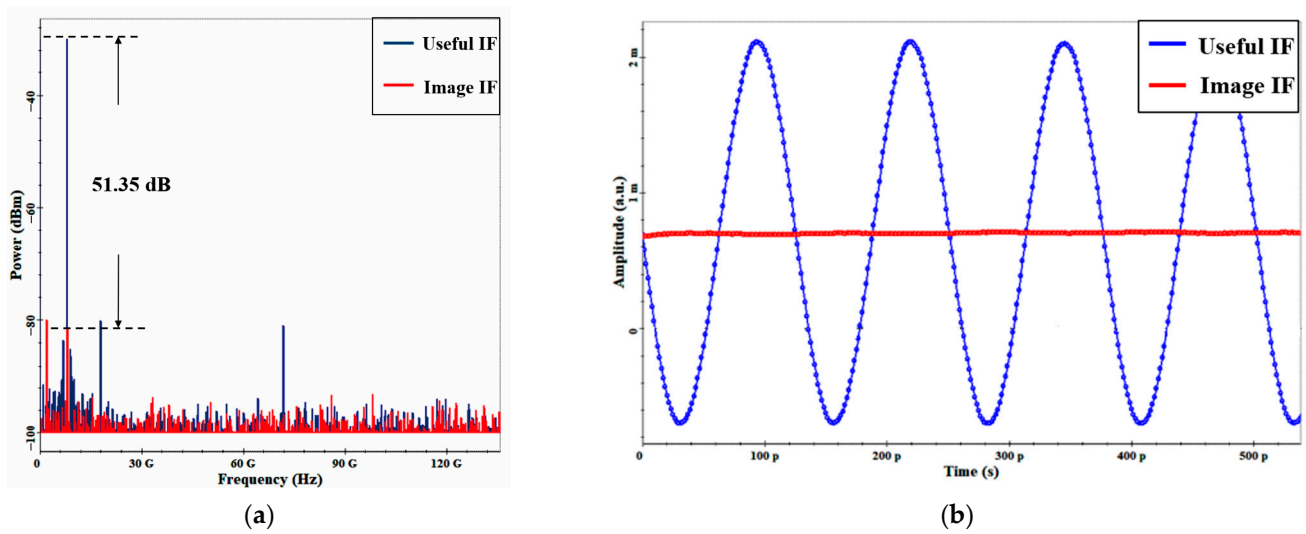


Figure 11. Measured spectra and waveforms of the down-conversion IF and image IF signals from the image-reject mixer. (a) IF signal frequency spectrum; (b) IF signal waveform.

Finally, the dynamic range of the proposed system is evaluated by measuring its SFDR. The frequency of the LO signal is set to 5 GHz. A two-tone signal with frequencies of 18 GHz and 18.1 GHz is employed as the RF signal. The power of the two-tone RF signal is gradually increased from -2 to 6 dBm, and the power of the fundamental term and the third-order intermodulation distortions (IMD3) are recorded. The results are presented in Figure 12. Assuming that the noise floor is -160 dBm/Hz, the SFDR of the up-conversion and down-conversion are 97 dB·Hz^{2/3} and 97.27 dB·Hz^{2/3}, respectively.

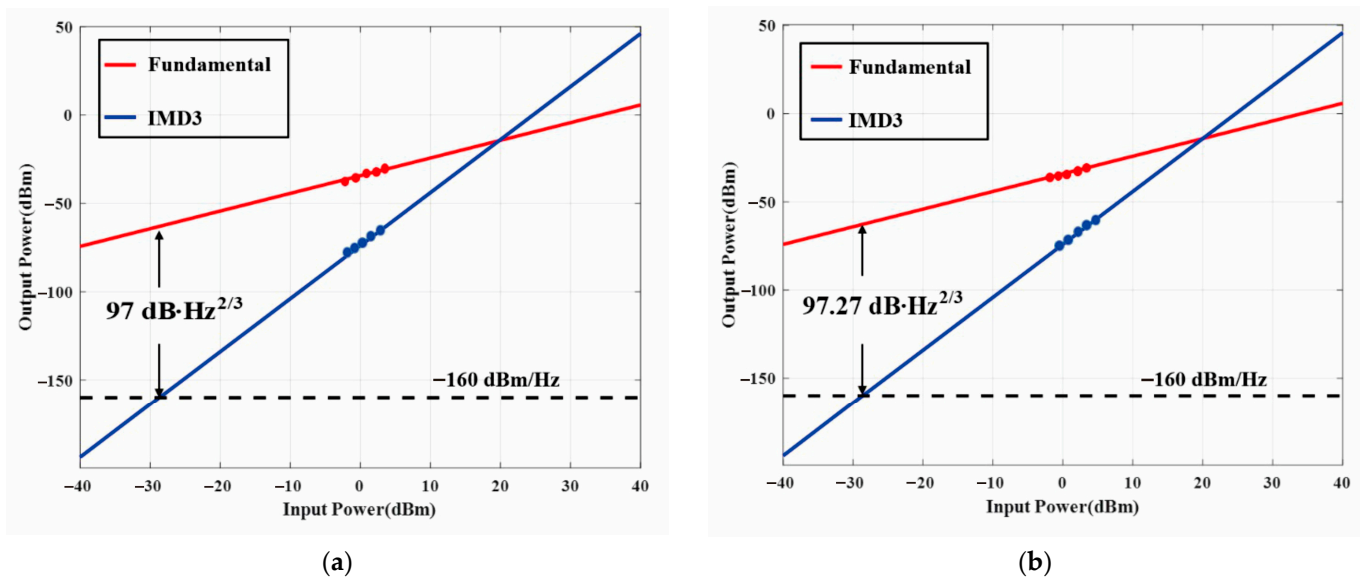


Figure 12. The SFDR of the reconfigurable LO harmonic mixer. (a) Second-order LO harmonic up-conversion; (b) second-order LO harmonic down-conversion.

4. Discussion

Photonics-based microwave frequency mixing has been reported in recent decades. For example, Zhu et al. proposed a frequency down-conversion scheme based on CS-SSB modulation via an integrated DP-MZM [19]. Shen and Zhou proposed a dual parallel in- an I/Q modulators-based microwave photonic mixer [10]. Considering frequency conversion efficiency, the above-mentioned solutions have their limitations since they can only achieve down-conversion of a single frequency and are only suitable for point-to-point

scenarios. In this paper, according to the simulation results, an OFC was generated using the sub-Y-DPMZM. By applying the OFC as a multi-carrier light source, this scheme can be extended to multi-channel and multi-band systems, thus generating signals in different frequency bands to meet the demands of various satellite communication services. Previous proposed schemes usually contain more than one optical modulator. For example, Kong et al. presented a flexible microwave photonic image-reject mixer, including two MZMs and one PM in the scheme [20]. Lee and Song experimentally demonstrated a photonic frequency down-converter based on an optoelectronic oscillator using two cascaded electro-absorption modulators [21]. Compared to the existing schemes, our scheme only utilizes a single PDM-DPMZM for frequency mixing, which makes it easier to adjust the parameters during the reconfiguration process. It will also contribute to a more compact overall structure, lower system complexity, and improved reliability.

Furthermore, the proposed scheme utilized MZM and PDs to achieve electro-optical and optical-electrical conversion, completing the processing of RF signals in the optical domain. Compared to microwave mixers in the electrical domain [22–24], the proposed scheme utilized electromagnetic interference-resistant optical devices to enhance the resilience of the system against the harsh space radiation environment, minimizing the risk of component failures. Meanwhile, the frequency conversion system implemented image rejection capabilities to eliminate the impact of IM on the mixing process, thereby enhancing the system's anti-interference ability to respond to varying interference sources in the space spectrum. Finally, compared to non-reconfigurable solutions [9–12], the scheme proposed in this paper is more flexible. It can be switched to select the up-conversion or down-conversion and enables the flexible selection of \pm first, \pm second, \pm third, \pm fourth-order sidebands of the LO for mixing according to specific requirements, thereby achieving signal output in different frequency bands. Moreover, the WSS can independently switch any frequency gap in the optical signal to the output port, and the WSS is fully reconfigurable as an optical filter, which makes the proposed scheme more flexible in its application in different scenarios.

The currently proposed scheme is built by discrete devices, and the insertion loss introduced by discrete devices can affect the performance of the system. In subsequent studies, it will be better to use microwave photonic integrated devices instead of discrete devices to reduce the size, decrease the loss and improve the reliability of the scheme.

5. Conclusions

In conclusion, a reconfigurable LO harmonic mixer with simultaneous phase shifting and image rejection is proposed and verified. This mixer can utilize four different LO harmonic sidebands to achieve the frequency mixing of signals in different frequency bands, covering a wider range of bands. The phase can be continuously tuned within the range of 0 to 360°, with a flat amplitude response. By adjusting the angle of Pol, it can compensate the inherent phase deviation of a 90° electrical hybrid coupler and achieve better image-rejection performance. Through building a simulation system, we verified the multi-band frequency conversion, continuous phase tunability, and image rejection of the proposed mixer. Under the conditions of the second-order LO harmonic down-conversion mode, the conversion gain reached above –35 dB, with SSR exceeding 46 dB. The IRR reached 51.35 dB, which is approximately 5 dB higher than that in existing schemes. When the LO signal power is 18 dBm, the NF is approximately 40 dB. In the case of second-order LO harmonic down-conversion mode, the SFDR is 97.27 dB·Hz^{2/3}.

The proposed frequency mixing scheme enables flexible frequency conversion for bands such as Ka/Q/V. To withstand the unique challenges of space, such as harsh space radiation and varying interference sources in the space spectrum, we adopted a photonics-based microwave frequency mixing scheme. Processing multi-band signal convergence in S-IoT networks in the optical domain is a potential future direction for on-board payloads. The proposed scheme is constructed with discrete devices, which can also be replaced

by integrated devices in the future to further enhance the efficiency, reliability and anti-interference of the system.

Author Contributions: Conceptualization, B.W.; methodology, B.W. and C.Z.; investigation, B.W., C.Z., H.Z. and Q.Z.; writing—original draft preparation, B.W. and C.Z.; writing—review and editing, B.W., C.Z., H.Z. and Q.Z.; All authors have read and agreed to the published version of the manuscript.

Funding: This work is supported in part by the National Science Foundation of China (NSFC) under Grant 62101113, China; the Natural Science Foundation of Hebei Province under Grant F2020501035; the Fundamental Research Funds for the Central Universities under Grant N2023008 and N2123024.

Data Availability Statement: The data presented in this paper are available after contacting the corresponding author.

Conflicts of Interest: The authors declare no conflicts of interest.

References

- Jiao, J.; Wu, S.H.; Lu, R.X.; Zhang, Q.Y. Massive access in space-based Internet of Things: Challenges Opportunities, and Future Directions. *IEEE Wirel. Commun.* **2021**, *5*, 118–125. [\[CrossRef\]](#)
- Tang, Z.Z.; Li, Y.F.; Yao, J.P.; Pan, S.L. Photonics-based microwave frequency mixing: Methodology and applications. *Laser Photon. Rev.* **2020**, *14*, 1800350. [\[CrossRef\]](#)
- Li, H.; Zhao, S.H.; Lin, T.; Zhang, K.; Jiang, W.; Wang, G.D.; Li, X. A filterless reconfigurable frequency mixer based on a wideband photonic microwave phase shifter. *Opt. Commun.* **2020**, *475*, 126224. [\[CrossRef\]](#)
- Jia, P.R.; Ma, J.X. Dual-Output Microwave Photonic Frequency Up- and Down-Converter Using a 90° Optical Hybrid Without Filtering. *IEEE Photonics J.* **2022**, *14*, 5534208. [\[CrossRef\]](#)
- Huang, L.; Li, R.M.; Chen, D.L.; Xiang, P.; Wang, P.; Pu, T.; Chen, X.F. Photonic Downconversion of RF Signals with Improved Conversion Efficiency and SFDR. *IEEE Photonics Technol. Lett.* **2016**, *28*, 880–883. [\[CrossRef\]](#)
- Atzori, L.; Iera, A.; Morabito, G. The Internet of Things: A survey. *Comput. Netw.* **2010**, *54*, 2787–2805. [\[CrossRef\]](#)
- Ghelfi, P.; Laghezza, F.; Scotti, F.; Serafino, G.; Capria, A.; Pinna, S.; Onori, D.; Porzi, C.; Scaffardi, M.; Malacarne, A.; et al. A fully photonics-based coherent radar system. *Nature* **2014**, *507*, 341–345. [\[CrossRef\]](#) [\[PubMed\]](#)
- Pan, S.L.; Zhu, D.; Liu, S.F.; Xu, K.; Dai, Y.T.; Wang, T.L.; Liu, J.G.; Zhu, N.H.; Xue, Y.; Liu, N.J. Satellite payloads pay off. *IEEE Microw. Mag.* **2015**, *16*, 61–73. [\[CrossRef\]](#)
- Li, J.N.; Wang, Y.X.; Wang, D.Y.; Zhou, T.; Xu, J.H.; Zhong, X.; Yang, F.; Yang, D.C.; Rong, L. A Microwave Photonic Mixer Using a Frequency-Doubled Local Oscillator. *IEEE Photonics J.* **2018**, *10*, 5501210. [\[CrossRef\]](#)
- Shen, G.; Zhou, Y. Broadband Microwave Photonic Mixer with High Spurs Suppression and Image Rejection. *IEEE Photonics J.* **2024**, *16*, 5500108. [\[CrossRef\]](#)
- Chen, H.; Chan, E.H.W. Microwave Photonic I/Q Mixer with Phase Shifting Ability. *IEEE Photonics J.* **2021**, *13*, 7100707. [\[CrossRef\]](#)
- Tang, Z.Z.; Pan, S.L. Image-Reject Mixer with Large Suppression of Mixing Spurs Based on a Photonic Microwave Phase Shifter. *J. Light. Technol.* **2016**, *34*, 4729–4735. [\[CrossRef\]](#)
- Lin, T.; Zhang, Z.K.; Liu, J.G.; Zhao, S.H.; Li, J.Y.; Zou, C.W.; Wang, J.J.; Zhang, K.; Jiang, W. Reconfigurable Photonic Microwave Mixer with Mixing Spurs Suppressed and Dispersion Immune for Radio-Over-Fiber System. *IEEE Trans. Microw. Theory Tech.* **2020**, *68*, 5317–5327. [\[CrossRef\]](#)
- Li, T.; Chan, E.H.W.; Wang, X.D.; Feng, X.H.; Guan, B.; Yao, J.P. Broadband Photonic Microwave Signal Processor with Frequency Up/Down Conversion and Phase Shifting Capability. *IEEE Photonics J.* **2018**, *10*, 5500112. [\[CrossRef\]](#)
- Zhang, Y.M.; Li, Z.Y.; Chen, W.J.; Liu, C.; Shao, K.L.; Zhu, D.; Pan, S.L. Broadband Image-Reject Mixing Based on a Polarization-Modulated Dual-Channel Photonic Microwave Phase Shifter. *IEEE Photonics J.* **2020**, *12*, 7800409. [\[CrossRef\]](#)
- Gao, Y.S.; Wen, A.J.; Jiang, W.; Fan, Y.Y.; He, Y. All-optical and broadband microwave fundamental/sub-harmonic I/Q down-converters. *Opt Express* **2018**, *26*, 7336–7350. [\[CrossRef\]](#) [\[PubMed\]](#)
- Shi, Z.; Zhu, S.; Li, M.; Zhu, N.H.; Li, W. Reconfigurable microwave photonic mixer based on dual-polarization dual-parallel Mach-Zehnder modulator. *Opt. Commun.* **2018**, *428*, 131–135. [\[CrossRef\]](#)
- Tang, Z.Z.; Pan, S.L. Reconfigurable microwave photonic mixer with minimized path separation and large suppression of mixing spurs. *Opt. Lett.* **2017**, *42*, 33–36. [\[CrossRef\]](#)
- Zhu, Z.H.; Zhao, S.H.; Li, X.; Lin, T.; Zhang, K. High performance photonic microwave frequency down-conversion using a dual-drive dual-parallel Mach-Zehnder modulator. *J. Mod. Opt.* **2018**, *66*, 143–152. [\[CrossRef\]](#)
- Kong, X.; Yu, Y.; Tang, H.T.; Zhang, X.L. Microwave Photonic Image-Reject Mixer Based on a Tunable Microwave Photonic Filter With High Rejection. *IEEE Photonics J.* **2018**, *10*, 5502411. [\[CrossRef\]](#)
- Lee, J.-Y.; Song, J.-I. Photonic Frequency Down-Converter Based on a Frequency-Doubling OEO Using Two Cascaded EAMs. *IEEE Photonics Technol. Lett.* **2017**, *29*, 1529–1532. [\[CrossRef\]](#)

22. Mohammad, A.; Balakier, K.; Shams, H.; Van Dijk, F.; Liu, C.; Graham, C.; Natrella, M.; Lin, X.; Seeds, A.; Renaud, C. 60 GHz Wireless Link Implementing an Electronic Mixer Driven by a Photonically Integrated Uni-Traveling Carrier Photodiode at the Receiver. In Proceedings of the 2018 International Topical Meeting on Microwave Photonics (MWP), Toulouse, France, 22–25 October 2018; pp. 1–4.
23. Lee, I.; Kim, S. H-band down-conversion and up-conversion mixers with wide IF bandwidth. In Proceedings of the 2016 IEEE MTT-S International Microwave Symposium (IMS), San Francisco, CA, USA, 22–27 May 2016; pp. 1285–1296.
24. Wang, Z.H.; Chen, C.N.; Huang, T.W.; Wang, H. A 28-GHz High Linearity Up-Conversion Mixer Using Second-Harmonic Injection Technique in 28-nm CMOS Technology. *IEEE Microw. Wirel. Compon. Lett.* **2021**, *31*, 276–279. [[CrossRef](#)]

Disclaimer/Publisher’s Note: The statements, opinions and data contained in all publications are solely those of the individual author(s) and contributor(s) and not of MDPI and/or the editor(s). MDPI and/or the editor(s) disclaim responsibility for any injury to people or property resulting from any ideas, methods, instructions or products referred to in the content.